

# Testing of a 40-kW<sub>th</sub> Counterflow Particle-Supercritical Carbon Dioxide Narrow-Channel, Fluidized Bed Heat Exchanger

Winfred J. Arthur-Arhin<sup>1</sup>[\[https://orcid.org/0000-0003-2045-1733\]](https://orcid.org/0000-0003-2045-1733), Jesse R. Fosheim<sup>1</sup>[\[https://orcid.org/0000-0001-7794-3558\]](https://orcid.org/0000-0001-7794-3558), Keaton J. Brewster<sup>1</sup>[\[https://orcid.org/0000-0002-3307-3228\]](https://orcid.org/0000-0002-3307-3228), Azariah Thompson<sup>1</sup>, , Kevin J. Albrecht<sup>2</sup>, Dereje Amogne<sup>3</sup>[\[https://orcid.org/0009-0007-4675-6726\]](https://orcid.org/0009-0007-4675-6726), and Gregory S. Jackson<sup>1</sup>[\[https://orcid.org/0000-0002-8928-2459\]](https://orcid.org/0000-0002-8928-2459)

<sup>1</sup> Colorado School of Mines, Golden, CO

<sup>3</sup> Sandia National Laboratories, Albuquerque, NM

<sup>3</sup> Vacuum Process Engineering, Inc. Sacramento, CA

**Abstract.** Particle-based primary heat exchangers (HXs) must deliver sCO<sub>2</sub> fluid temperatures above 700°C to couple particle-based concentrating solar receivers and thermal energy storage (TES) sub-systems with efficient sCO<sub>2</sub> power cycles. Particle-sCO<sub>2</sub> HX designs have struggled to meet DOE cost targets ( $\leq \$150/\text{kW}_{\text{th}}$ ) due to the amount of expensive nickel alloys necessary for manufacturing full-scale, particle-sCO<sub>2</sub> HXs. Our team has demonstrated that mild bubbling fluidization of falling particles in a counterflow narrow-channel fluidized bed can reduce required HX surface area and thus, costs by increasing particle-wall heat transfer coefficients  $h_{T,w} > 800 \text{ W m}^{-2} \text{ K}^{-1}$ . This paper reports on the fabrication and testing of a stainless steel, particle-sCO<sub>2</sub> HX with 12 fluidized-bed channels approximately 10.5 mm deep spaced between diffusion-bonded, micro-channel sCO<sub>2</sub> plates. The HX with a core length of  $\approx 0.56 \text{ m}$  is fed with CARBOBEAD HSP particles through a short, fluidized freeboard zone just above the core. Testing to date in the National Solar Thermal Test Facility (NSTTF) at Sandia National Laboratories has shown that parallel bed fluidization maintains uniform particle inventory across the instrumented channels. Heat transfer thermal duty between the particle and sCO<sub>2</sub> flows exceeds 30 kW<sub>th</sub> with sCO<sub>2</sub> inlet temperatures of 200°C and particle inlet temperatures up to 440°C and mass flow rates of 0.2 kg s<sup>-1</sup> fluidized by counterflowing gas flow rates of 0.005 kg s<sup>-1</sup>. Tests at higher particle and sCO<sub>2</sub> inlet temperatures (600°C and 400°C respectively) are targeted to achieve  $> 40 \text{ kW}_{\text{th}}$  with model-predicted overall heat transfer coefficients  $U > 400 \text{ W m}^{-2} \text{ K}^{-1}$ .

**Keywords:** Concentrating Solar Power, Particle Heat Exchangers, Fluidized Bed Heat Transfer

## 1. Introduction

Coupling next-generation, particle-based concentrating solar receivers and thermal energy storage (TES) sub-systems with efficient supercritical-CO<sub>2</sub> (sCO<sub>2</sub>) power cycles such as the recompression-closed Brayton cycle (RCBC) has the potential to provide 24/7 dispatchable electricity from intermittent solar energy [1]. Integrating central tower receivers with sCO<sub>2</sub> power cycles requires particle-sCO<sub>2</sub> heat exchangers that deliver sCO<sub>2</sub> fluid temperatures above 700°C [2, 3]. Engineered oxide particles such as CARBOBEAD HSP can be stored at adequately high temperatures ( $> 800^\circ\text{C}$ ) to drive these sCO<sub>2</sub> cycles, but primary heat exchanger designs based on narrow-channel, moving-packed bed heat exchangers [4, 5] are

challenged by high costs per  $\text{kW}_{\text{th}}$  because of the required surface area of expensive high-temperature alloys due to the dominant thermal resistance associated with particle-wall heat transfer coefficients  $h_{\text{T,w}}$ .

To reduce the thermal resistance associated with particle-wall heat transfer, some researchers, including our team, have been exploring bubbling fluidization in particle heat exchanger beds [6, 7]. The unique approach adopted here for fluidization involves counterflow, narrow-channel bubbling beds [8], which at relatively low gas-to-particle mass flow ratios ( $\dot{m}_{\text{g}}/\dot{m}_{\text{p}} < 2.5\%$ ), can more than double  $h_{\text{T,w}}$  relative to moving packed beds for the same particle bed depth [9]. However, questions remain about the stability of multi-channel bed fluidization and the parasitic losses associated with providing fluidizing gas in heat exchanger flow-paths. The single-channel tests provided a basis for developing a correlation for  $h_{\text{T,w}}$  following the approach of Molerus [9, 10], and the correlation is implemented into a 1-D multi-phase flow model for narrow-channel, fluidized beds. The fluidized bed sub-model is incorporated into a reduced-order, vertically discretized numerical model of a fluidized-bed particle- $\text{sCO}_2$  heat exchanger that incorporates thermal wall conduction, and a microchannel  $\text{sCO}_2$  flow sub-model [5].

A numerical parametric study using the fluidized bed, narrow-channel particle- $\text{sCO}_2$  heat exchanger model explored the impacts of channel geometry and operating conditions on overall performance metrics to identify heat exchanger design and operating conditions to provide 40  $\text{kW}_{\text{th}}$  thermal duty for  $\text{sCO}_2$  flows entering the heat exchanger at  $\dot{m}_{\text{CO}_2} = 0.2 \text{ kg s}^{-1}$  at  $T_{\text{sCO}_2,\text{in}} = 400^\circ\text{C}$  and particle inlet temperatures of  $T_{\text{p,in}} = 600^\circ\text{C}$  [11]. The resulting particle- $\text{sCO}_2$  heat exchanger core design for inlet particle temperatures  $T_{\text{p,in}} = 600^\circ\text{C}$  has 12-parallel fluidized beds between two plates of microchannel- $\text{sCO}_2$  flows per bed. This heat exchanger was fabricated from 316 stainless steel plates with the microchannels fabricated via electrochemical etching and Vacuum Process Engineering's (VPE's) proprietary diffusion bonding process. The heat exchanger is integrated with a rotating-scoop inlet particle flow control, a freeboard zone above the core for gas-particle separation, and an outlet hopper. After room-temperature tests at Mines to assess the evenness of particle filling and fluidization, the heat exchanger was moved to Sandia National Laboratories (SNL) where the recently enhanced particle and  $\text{sCO}_2$  flow loops of the National Solar Thermal Test Facility (NSTTF) enable testing to particle inlet temperatures and  $\text{sCO}_2$  pressure at or beyond the design conditions. To date, preliminary heat exchanger tests at intermediate temperatures provide confidence that parallel fluidized beds in narrow channels can be sustained with reliable multi-channel flow distribution and controlled inventory at high solid-volume fractions. Environmental results demonstrate a pathway for robust operation of the heat exchanger with high-heat fluxes and reduced surface area heat exchangers for coupling particle-based TES subsystems to  $\text{sCO}_2$  power cycles. Successful demonstration of the 40- $\text{kW}_{\text{th}}$  particle- $\text{sCO}_2$  heat exchanger with increased overall  $U$  relative to moving packed bed heat exchangers can provide critical direction for scaling up fluidized bed particle- $\text{sCO}_2$  heat exchangers for next-generation CSP plants.

## 2. Heat Exchanger Design and Fabrication

The heat exchanger design was derived from a reduced-order, vertically discretized, quasi-1D model of the particle- $\text{sCO}_2$  heat exchanger core that couples a multi-phase, fluidized-bed sub model with thermal wall conduction and a microchannel  $\text{sCO}_2$  flow sub-model [11]. At the design conditions of  $T_{\text{p,in}} = 600^\circ\text{C}$ , the model indicated that a stainless-steel heat exchanger, can transfer over 40  $\text{kW}_{\text{th}}$  from the falling fluidized particles to the upward  $\text{sCO}_2$  flow in 12 parallel

channels with a core height  $\Delta y_b = 0.4$  m, bed depth  $\Delta z_b = 10.5$  mm, and bed width  $\Delta x_b = 0.2$  m. The design (40-kW<sub>th</sub>) and tested conditions to date are shown in Table 1.

For the sCO<sub>2</sub> flow, the heat exchanger incorporated unique microchannels in the heat transfer plate walls designed by VPE. Two sets of microchannels on opposite sides of each fluidized

**Table 1.** Stainless-steel fluidized bed particle-sCO<sub>2</sub> heat exchanger design flow conditions for testing at the National Solar Thermal Test Facility.

HX Flows	Property	Tested conditions	Design test conditions
<b>CARBOBEAD HSP particles</b>	mean diam. $d_p$	287 $\mu\text{m}$	360 $\mu\text{m}$
	bulk density $\rho_p$	3610 $\text{kg m}^{-3}$	3610 $\text{kg m}^{-3}$
	inlet temp., $T_{p,\text{in}}$	400°C	600°C
	mass flow rate, $\dot{m}_p$	200 $\text{g s}^{-1}$	200 $\text{g s}^{-1}$
<b>fluidizing air</b>	inlet temp., $T_{g,\text{in}}$	200°C	400°C
	mass flow rate, $\dot{m}_g$	< 5.0 $\text{g s}^{-1}$	2.0 to 4.0 $\text{g s}^{-1}$
<b>supercritical CO<sub>2</sub></b>	inlet temp., $T_{\text{sCO}_2,\text{in}}$	200°C	400°C
	mass flow rate, $\dot{m}_{\text{sCO}_2}$	200 $\text{g s}^{-1}$	200 $\text{g s}^{-1}$
	inlet pressure, $P_{\text{sCO}_2,\text{in}}$	17 MPa	17 MPa

bed (i.e., 24 microchannel plates for 12 parallel fluidized beds) were electrochemically etched into diffusion -bonded 316 stainless steel plates to provide very high heat transfer rates ( $h_{T,\text{sCO}_2,\text{eff}} \approx 2000 \text{ W m}^{-2} \text{ K}^{-1}$ ) due to the small dimensions with single channel hydraulic diameter of 0.75 mm. The sCO<sub>2</sub> plates have unique manifolds both above and below the vertical microchannels to distribute the sCO<sub>2</sub> from inlet headers that provide fluid from both sides of the bottom core as shown in the assembly drawing and photograph in Figs. 1a and 1b respectively. A similar manifold in the micro-channel plates at the top of the core allows the heated sCO<sub>2</sub> to exit through two outlet headers as depicted in Fig. 1a. The manifolds add  $\approx 8$  cm at both the bottom and top of the heat exchange surface area between the particle bed channels and the sCO<sub>2</sub> flows such that the actual core height extends to 0.555 m. With the fluidized bed width  $\Delta x_b = 0.2$  m, an overall wall heat transfer area  $A_{w,\text{tot}} = 0.110 \text{ m}^2$  per wall \* 24 walls = 2.64  $\text{m}^2$  is used to calculate overall heat transfer coefficients  $U$  for the heat exchanger.

Air injection for each fluidized bed channel occurs through individual tubes with outer diameters  $d_{\text{tube}} = 6.35$  mm with two rows of 500 injector holes with diameter of 127  $\mu\text{m}$ . The air injector tubes are staggered between neighboring beds at heights of 0.086 m and 0.102 m from the base of the heat exchanger core. To achieve uniform fluidization in all 12 channels, a common air manifold feeds the injector tubes and maintains a low pressure drop across the internal passage of each injector tube. The region below the injector tubes has particle flow that resembles a moving packed bed and is approximately 17% of the core bed height. Although recent demonstration tests of moving packed bed particle heat exchangers have indicated relatively high overall  $U$  approaching 500  $\text{W m}^{-2} \text{ K}^{-1}$ , these were achieved with much thinner particle beds  $\Delta z_b = 3.0$  mm [12]. With the thicker beds here, particle-wall  $h_{T,w}$  in the moving packed bed region of the core is expected to be significantly lower as indicated by single-channel test experiments at Mines [9].

High  $h_{T,w}$  are expected in the fluidized bed region based on a convective Nusselt number correlation derived from extensive testing of narrow-channel fluidized beds in a 0.25 m high single-channel heat transfer rig at the Colorado School of Mines [9]. The correlation captures the experimental observation that  $h_{T,w}$  peaks at relatively mild fluidization conditions where the superficial gas velocity  $U_g$  is approximately 4-5 times the minimum fluidization velocity  $U_{\text{mf}}$  at  $T_p = 400^\circ\text{C}$ . For the CARBOBEAD HSP 45/60 particles (mean diameter  $d_p = 287 \mu\text{m}$  and bulk density  $\rho_p = 3610 \text{ kg m}^{-3}$ ) used in heat exchanger tests in this study,  $U_{\text{mf}} \approx 0.074 \text{ m s}^{-1}$  at  $T_p = 400^\circ\text{C}$ , and a relatively low  $U_g \approx 0.32 \text{ m s}^{-1}$  supports a near maximum  $h_{T,w} \approx 700 \text{ W m}^{-2} \text{ K}^{-1}$ .

However, it should be noted that this higher  $h_{T,w}$  only occurs in the fluidized regions of the bed above the injectors.

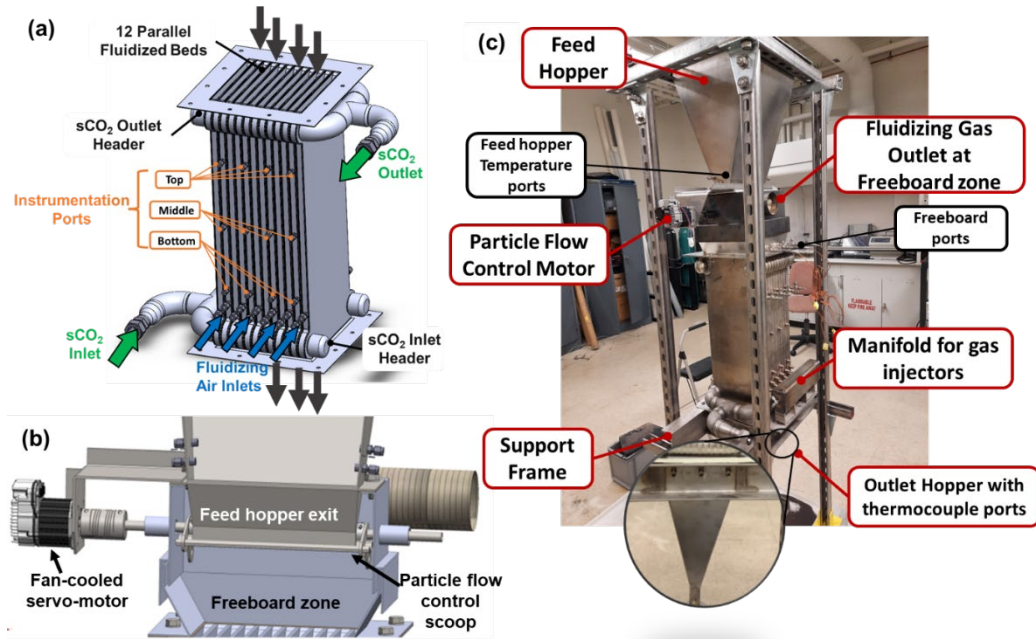


**Figure 1.** a) Assembly drawing of 40-kW<sub>th</sub> fluidized-bed, particle-sCO<sub>2</sub> heat exchanger core showing inlet and outlet flows and instrumentation ports in four channels for bed temperature and gas pressure measurements. b) assembly drawing of section of freeboard zone and rotating particle scoop for flow control, and c) photograph for room temperature fluidization testing of fluidized-bed heat exchanger assembled with particle feed hopper, rotating scoop for inlet particle flow control, freeboard zone for gas-particle separation, and particle outlet hopper.

Novel particle-inlet-flow control is implemented to provide uniform particle feed into the freeboard zone above the multiple parallel fluidized bed channels in the core. The flow control includes an angled scoop supported between side plates that is rotated through a displaced shaft by a servo motor to regulate particle flow over the edge of the scoop. This rotary scoop mechanism, shown in the assembly drawing in Figure 1b, relies on the fact that particles support themselves at the angle of repose to seal at the exit slot of the feed hopper. Because the mechanism actuates particle flow along a line as shown in Figure 1b, particles are fed into the freeboard zone as a falling curtain that spans across the parallel fluidized bed channels. The rotary scoop at its maximum opening in combination with the feed hopper exit slot supports over 0.5 kg s<sup>-1</sup> of particle flow with CARBOBEAD HSP, which is well above the design  $\dot{m}_p = 0.2 \text{ kg s}^{-1}$ .

The freeboard zone above the core of the heat exchanger provides a region of expanded area to lower the effective local  $U_g$  at the top of the core where the particles enter and the gas exits. Mild fluidization in the freeboard zone spreads particles over the full cross section of the heat exchanger core entrance. Because of the increased cross-sectional area in the freeboard zone, the very mild fluidization in the freeboard zone region above the core supports passive particle-gas separation allowing the fluidizing air to exit above the freeboard zoned through a thin, porous media mesh into the exhaust air ducting.

The heat exchanger instrumentation includes six K-type thermocouples near the exit of the feed hopper, which measure  $T_{p,in}$  and six K-type thermocouples just below the heat exchanger core for the outlet particle temperature  $T_{p,out}$ . Within the bed 4 of the 12 channels (channel # 2, 5, 8 and 11) were instrumented with ports that allows both local pressure and bed temperature measurements in three height locations in the bed labeled bottom ( $\Delta y_{\text{bottom}} = 0.138 \text{ m}$ ),

middle ( $\Delta y_{\text{middle}} = 0.288 \text{ m}$ ), and top ( $\Delta y_{\text{top}} = 0.438 \text{ m}$ ), where all heights are from the core outlet below the injectors. The pressure difference  $\Delta p_b$  between the three pressure taps provides a measure of the weight of the fluidized particles in that region which determines the average solid volume fraction  $\alpha_b$  when the bed is fluidized. Above the core in the freeboard zone, three pressure and temperature ports across the depth of the heat exchanger and located 0.017 m above the inlet to the core were used to track pressure drop due to the presence of particles above the port in the freeboard zone and their temperature  $T_{p,fb}$ . The drop in  $T_{p,fb}$  from the particle inlet  $T_{p,in}$  provides a measure for how much vertical particle dispersion in the narrow-channel beds lower the thermal driving force at the top of the bed as discussed below. The pressure measurement in the freeboard zone provides a basis for adjusting the particle inventory in the heat exchanger core by adjusting the angle of the rotary scoop valve. The particle flow through the heat exchanger core itself  $\dot{m}_p$  is set by the outlet of the bottom hopper which at the NSTTF test facility is provided by a motor-controlled sliding gate valve. Temperature measurements for the high-pressure  $\text{sCO}_2$  flow were provided upstream of the  $\text{sCO}_2$  inlet header for  $T_{\text{sCO}_2,in}$  and downstream of the  $\text{sCO}_2$  outlet header for  $T_{\text{sCO}_2,out}$ .

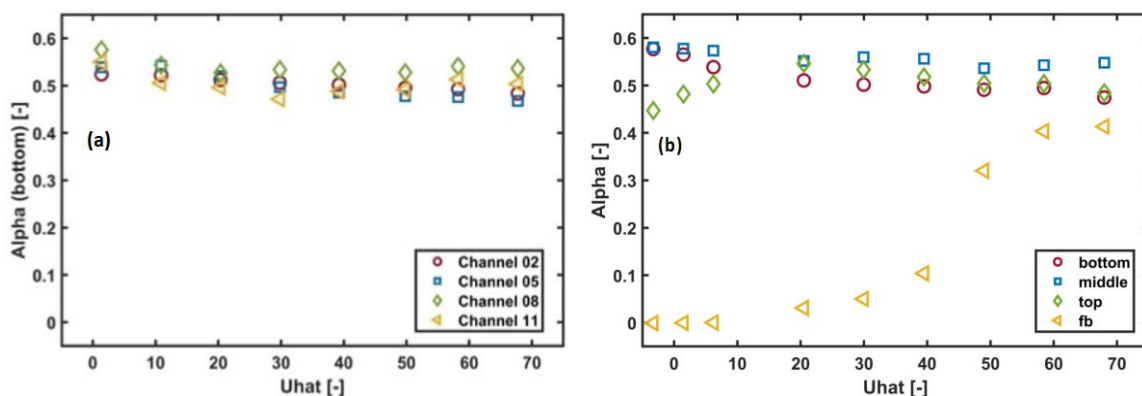
### 3. Heat Exchanger Tests

#### 3.1 Low Temperature Filling and Fluidization Tests

Before full-scale testing at elevated temperatures with  $\text{sCO}_2$  flow at NSTTF, Mines integrated the heat exchanger core, the particle feed hopper, inlet particle flow control with the freeboard zone, and the particle outlet hopper to do room-temperature shakedown testing of the particle fluidization. Because there was no ability at Mines to support continuous particle recycling, these tests were conducted in a batch mode with CARBOBEAD HSP 40/70 particles (mean  $d_p = 360 \mu\text{m}$ ). Visualization of fluidization tests in the freeboard zone above the heat exchanger core suggested no significant bias of the fluidization intensity across the length of the injectors or the depth of the bed. Fluidization in the room temperature batch mode tests explored how  $\alpha_b$  varied across the four instrumented channels and along their height as a function of the excess fluidization velocity  $U_g - U_{mf}$  which is characterized by the dimensionless  $\hat{U}$  in accordance with Molerus [10].

$$\hat{U} = (U_g - U_{mf})(\rho_p c_{p,p} / \lambda_g g)^{1/3} \quad (1)$$

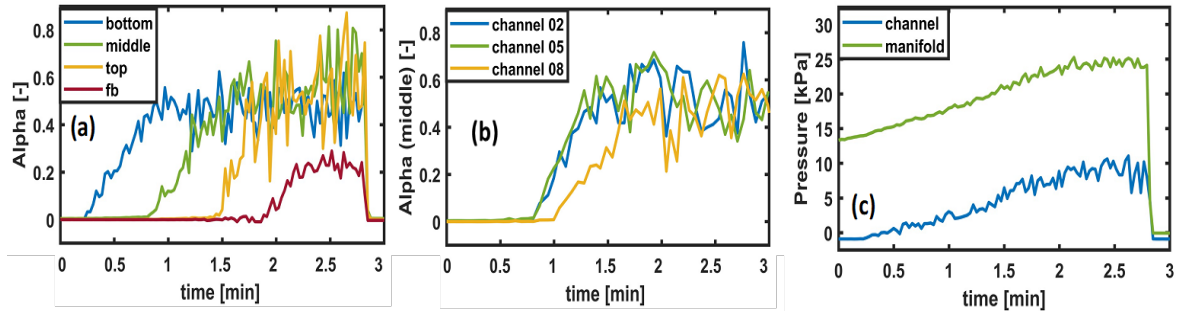
Figure 2a shows calculated  $\alpha_b$  from the measured  $\Delta p_b$  between the bottom port and the middle port vs.  $\hat{U}$  for the four channels during steady-state batch mode fluidization. The results show a slight decrease in  $\alpha_b$  with increasing  $\hat{U}$  up to 70 with overall mean  $\alpha_b$  for the entire bed remaining above 0.46, which is  $> 80\%$  of the maximum packing fraction of 0.585. The peak  $h_{T,w}$  with respect to  $\hat{U}$  occurs at  $\hat{U}$



**Figure 2.** a) Solid volume fractions  $\alpha_b$  determined from the mean pressure drop between the middle and bottom measurement ports in the particle heat exchanger core as a function of dimensionless excess fluidization velocity  $\hat{U}$  at room temperature. b) Variation in  $\alpha_b$  with  $\hat{U}$  in the bottom, middle, and top of the particle heat exchanger channel 5. The freeboard zone  $\alpha_b$  represents an average over a fixed height above the top of the particle bed and the rise in the freeboard zone  $\alpha_b$  indicates a rise in the height of the bed above the core.

Between 50 and 60, and thus, the results in Figure 2a indicate that particle inventory in the fluidized channel beds will not vary significantly during operation for high  $h_{T,w}$ . Figure 2b shows that the mean  $\alpha_b$  does not vary significantly over the height of the channels.  $\alpha_b$  for the freeboard zone presents the mean value over a fixed height that extends beyond the top of the particle bed, and the rise in the freeboard zone indicates a rise in the top of the fluidized region with increasing  $\hat{U}$ . Pressure drop in the freeboard zone provides a basis for assessing particle inventory in the freeboard zone and ensuring that the heat exchanger core particle inlet is completely covered in particles for relatively uniform particle flow through the channels. The slight difference in  $\alpha_b$  in the channels does not denote differences in the particle flowrate between the channels but variations in fluidization, likely caused by variations in flow rates due to manifolding, manufacturing tolerances for the fluidization orifices, variations in relative pressure drop across channels and possibly variation in channels tolerances from fabrication. The sensitivity of  $\hat{U}$  and  $\alpha_b$  to even the slightest of uncertainty make this level of uniformity impressive.

The room temperature experiments also tested the uniformity of filling the heat exchanger with continuous fluidization in order to assess risks associated with gas flow channeling in particular channels. Filling experiments at the design particle inlet flow rate of  $\dot{m}_p = 0.2 \text{ kg s}^{-1}$  and a gas flow with  $\hat{U} \approx 50$  with CARBOBEAD HSP 40/70 particles tracked the evolution of the  $\alpha_b$  as a function of time as illustrated in Figure 3a. The plots in Figures 3a and 3b show significant noise due to the intrinsic pressure variations in fluidized bed and can be smoothed out with a significant time averaging of the pressure measurements for calculating  $\alpha_b$ . Figure 3b well represent the filling in other channels, which indicates that the particle inlet flow design provides reliable filling of the heat exchanger.



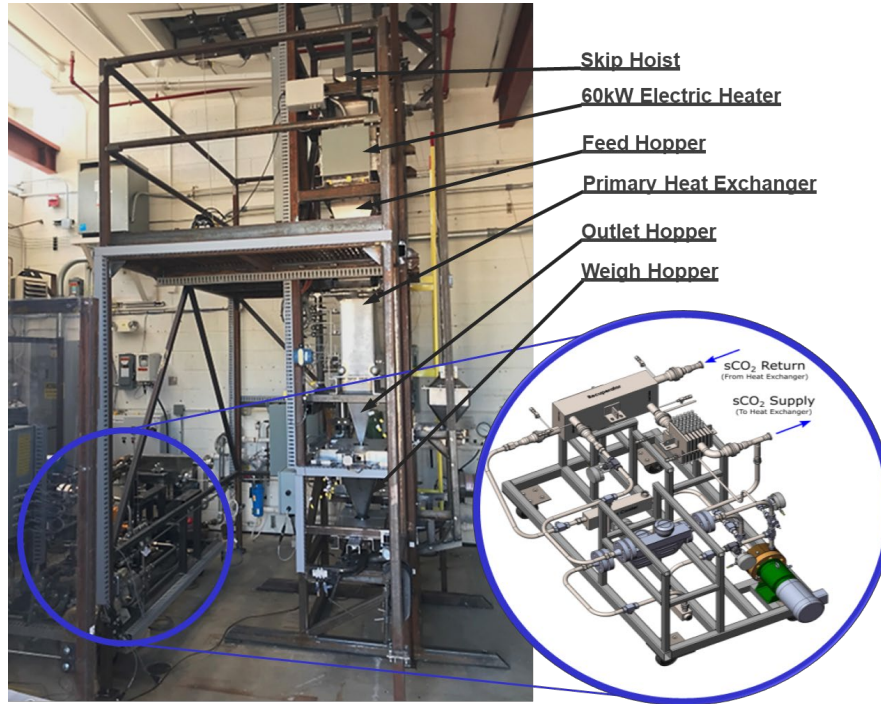
**Figure 3.** Plots of  $\alpha_b$  in a) channel 5 and b) bottom and middle ports of channels 2, channel 5 and, channel 8 during heat exchanger fill tests with  $\dot{m}_p = 0.2 \text{ kg s}^{-1}$  and constant  $\hat{U} \approx 50$ . Plots show rising particle inventory in different regions of the heat exchanger channels as the bed height rises into the freeboard (fb) zone above the bed. c) Evolution of pressure in the fluidizing gas manifold upstream of the injector (including injector and channel) and the bed channel as well as pressure in the bed channel downstream of the injector.

Figure 3c shows the evolution of the pressure in the air injector manifold and in the bottom channel of channel 5 during a filling experiment. The rise in the injector pressure is simply due to the increase in the pressure drop due to the particle bed. The large injector pressure drop across the injector of 13-15 kPa arises because of the small injector hole diameters and the high flow rates at room temperature due to the higher  $U_{mf}$ .  $\hat{U} \approx 50$  for CARBOBEAD HSP 40/70 at room temperature implies a  $U_g = 0.39 \text{ m s}^{-1}$ . The relatively small pressure drop through the full bed in Figure 3c shows that the dominant parasitic loads associated with fluidization will

likely be for the injector and not for the bed pressure drop for bed heights  $\Delta y_b < 1.0$  m.

### 3.2 Particle-sCO<sub>2</sub> Heat Exchanger Tests

The fluidized bed particle-sCO<sub>2</sub> heat exchanger was installed in the NSTTF heat exchanger test facility, which has been upgraded to provide the design flow rates and operating temperatures presented in the right column of Table 1. Recent NSTTF facility upgrades by Sandia include the installation of a vertical particle skip hoist for automated recycling of particles from the collection hopper back to the electric particle heater that provides heated gravity-driven particle flows to the feed hopper as shown in the facility photo in Figure 4. In addition, Sandia installed a recuperator and electric heater in the sCO<sub>2</sub> flow loop (as shown in the call out in



**Figure 4.** Labeled photograph of 40-kW<sub>th</sub> fluidized bed particle-sCO<sub>2</sub> heat exchanger installed in the test facility at NSTTF at Sandia National Laboratories showing the particle skip hoist, the upstream particle electric heater and the outlet and weigh hoppers for measuring mass flow. The improved sCO<sub>2</sub> flow loop is shown in the assembly drawing to the right.

Figure 4) that can provide reliably heat exchange inlets  $T_{sCO_2,in}$  up to 400°C. In addition, a new electronically controlled, pressured air supply with an electric heater supports fluidizing gas flows at temperatures  $T_{g,in}$  to 400°C for the fluidized bed heat exchanger tests.

Initial shakedown of the fluidized bed particle-sCO<sub>2</sub> heat exchanger at NSTTF revealed several challenges in setting up a fluidized bed heat exchanger. Initially, the design of the gas-particle separation above the heat exchanger allowed for horizontal air outlet passages with particle meshes. However, testing revealed the vertical meshes in the horizontal exhaust flows tended to collect particles and increase pressure within the freeboard zone. Thus, the team modified the air exhausts to turn upward, and place meshes in a horizontal direction such that stray particles in the air exhaust tend to fall back down into the freeboard zone. In general, the pressures in the heat exchanger as indicated in Figure 3b implies that air pressure in the bottom of the heat exchanger will find leaky passageways to the ambient including down through the outlet hopper exit. Significant efforts to increase sealing around joints to avoid undesired downward air flows as well as particle-laden air leaks mitigated these concerns. This included around a slip joint with ceramic insulation seal above the freeboard zone that permitted independent vertical growth of the heat exchanger and the heater and inlet feed hopper above the

heat exchanger. Observed minimum fluidization measurements in the heat exchanger suggested that almost all the air follows the intended flow path and passes up through the fluidized bed channels.

Low-temperature tests at the NSTTF indicated that the particle inventory could be sustained by monitoring the pressure-drop in the freeboard zone and adjusting the rotary inlet valve to supply particle flow rates into the freeboard zone that closely matched the particle flows out of the heat exchanger through the outlet valve. The need for two flow control valves differs from moving packed bed designs which only need a single particle flow control after the heat exchanger outlet hopper. The heat exchanger tests further confirmed the relatively uniform fluidization through the bed but now under conditions with downward particle flow rates.

To date, the highest temperature tests at NSTTF have been with  $T_{p,in}$  up to 440°C at the test conditions listed in the 3rd column of Table 1 including the use of smaller CARBOHSP 45/60 particles with mean  $d_p = 287 \mu\text{m}$ . These tests highlighted in Figure 5 and Table 2 vary the particle mass flow rate  $\dot{m}_p = 0.10 - 0.20 \text{ kg s}^{-1}$  whilst holding the  $\text{sCO}_2$  flow rate at  $\dot{m}_{\text{sCO}_2} = 0.20 \text{ kg s}^{-1}$  and the fluidizing gas flow rate at  $\dot{m}_g = 0.005 \text{ kg s}^{-1}$ . Figure 5a shows how the particle flow temperatures drop through the heat exchanger, from the feed hopper (particle inlet) to the top of the outlet hopper (particle outlet). In these tests, the particles heat up from  $T_{p,in} = 200^\circ\text{C}$  to  $400^\circ\text{C}$  at a low  $\dot{m}_p \approx 0.10 \text{ kg s}^{-1}$  for the first 90 min. Particle flow rate increases to  $\dot{m}_p \approx 0.15 \text{ kg s}^{-1}$  from the 90 min to 135 min, after which  $\dot{m}_p$  increases to  $0.20 \text{ kg s}^{-1}$ .

The large temperature difference between the feed hopper and the freeboard zone in Figure 5a is not due to heat loss as particles drop from the feed hopper into the freeboard zone, but rather is a result of the vertical dispersion of particles associated with fluidization bubbles that recirculate particles vertically as the bubbles rise and coalesce within the channels. The vertical mixing of recirculated particles with hotter particles falling into the freeboard zone from the feed hopper causes the measured temperature drop. The temperature difference of the particles between the particle feeder and the freeboard zone  $T_{p,in} - T_{p,fb}$  drops from  $\approx 100^\circ\text{C}$  at  $\dot{m}_{p,in} = 0.1 \text{ kg s}^{-1}$  to close to  $60^\circ\text{C}$  at  $\dot{m}_p = 0.2 \text{ kg s}^{-1}$  likely because the increased downward particle mass flux reduces the dispersion due to fluidization. The vertical temperature gradient  $\Delta T_p / \Delta y_b$  inside the fluidized region of the heat exchanger core actually increases with  $\dot{m}_p$  even with the higher heat capacity of the particle flow. This indicates how dispersion plays a larger impact on  $T_p$  at lower  $\dot{m}_p$ .

The overall heat transfer to the  $\text{sCO}_2$ ,  $\dot{Q}_{\text{sCO}_2}$  increases dramatically with  $\dot{m}_p$  as indicated in Table 2 rising from  $19.0 \text{ kW}_{\text{th}}$  to  $34.0 \text{ kW}_{\text{th}}$  as  $\dot{m}_p$  increases from  $0.1 \text{ kg s}^{-1}$  to  $0.2 \text{ kg s}^{-1}$ . The increase in  $\dot{Q}_{\text{sCO}_2}$  with  $\dot{m}_p$  is driven in part by the reduced dispersion and the increased log-mean temperature difference  $LMTD$ , but the overall  $U$  based on the  $LMTD$  and  $A_{w,tot}$  increases as well as shown in Table 2.

$$U = \dot{Q}_{\text{sCO}_2} / (A_{w,tot} LMTD) \quad (2)$$

The higher  $U$  with higher  $\dot{m}_p$  may be due in part to the increased  $T_p$  which will lead to higher  $h_{T,w}$  and thus  $U$ . This increase in  $U$  with  $\dot{m}_p$ , whilst maintaining  $\dot{m}_{\text{sCO}_2}$  however is less than proportional and thus lowers the heat exchanger effectiveness  $\varepsilon_{\text{HX}}$  down to 65% at the design  $\dot{m}_p$ . However, higher  $U$  at the design conditions (sweet spot) is expected to improve  $\varepsilon_{\text{HX}}$ .

Overall  $U$  values can be used to estimate an average particle-wall  $h_{T,w}$  in the narrow-channel beds (which includes both the fluidized region and the packed bed beneath the injectors).

$$h_{T,w} \approx [1/U - \Delta z_w / k_w - 1/h_{T,\text{sCO}_2,\text{eff}}]^{-1} \quad (3)$$

From values in Table 2, average particle wall  $h_{T,w}$  is estimated using an effective  $h_{T,\text{sCO}_2,\text{eff}} = 2000 \text{ W m}^{-2} \text{ K}^{-1}$  based on VPE's design. For  $U = 227 \text{ W m}^{-2} \text{ K}^{-1}$  at  $\dot{m}_p = 0.2 \text{ kg s}^{-1}$ , the estimate

according to eq. 2 for  $h_{T,w} = 325 \text{ W m}^{-2} \text{ K}^{-1}$  for the heat exchanger narrow channels. This value is lower than those observed from the smaller scale tests at Mines at similar conditions. This may in part be because of the 17% of  $A_{w,tot}$  exposed to a moving packed bed. Eq. 2 indicates that  $U = 650 \text{ W m}^{-2} \text{ K}^{-1}$  when  $h_{T,w}$  meets the target value of  $1000 \text{ W m}^{-2} \text{ K}^{-1}$  [9].

**Table 2.** Summary of particle-sCO<sub>2</sub> counterflow fluidized bed heat exchanger test results at near steady-state conditions for different particle flow rates.

$\dot{m}_p$ [g s <sup>-1</sup> ]	$\dot{m}_{sCO_2}$ [g s <sup>-1</sup> ]	$\dot{m}_g$ [g s <sup>-1</sup> ]	$T_{p,in}/T_{p,out}$ [°C]	$T_{CO_2,in}/T_{CO_2,out}$ [°C]	LMTD [°C]	$\dot{Q}_{sCO_2}$ [kW <sub>th</sub> ]	Overall $U$ [W m <sup>-2</sup> K <sup>-1</sup> ]	$\epsilon_{HX}$ [-]
100	200	5	400 / 210	200 / 300	44.3	19.0	157	0.83
150	200	5	420 / 235	200 / 315	63.7	28.0	202	0.76
200	200	5	435 / 260	200 / 340	76.2	34.0	227	0.65

Figure 5c plots the magnitude of enthalpy transfers to/from the three flows – particle, sCO<sub>2</sub>, and fluidizing air. The energy transfers show that when the heat exchanger approaches steady state conditions, the energy balance in the heat exchanger closes to within 5 to 8% with approximately 2% of the particle heat loss going to fluidizing air flow. It is expected that future longer duration tests will reach steady state conditions and provide a tighter energy balance. All the same, these confirms the expectation that the fluidizing gas will take only a small fraction of heat from the sCO<sub>2</sub> flow with the expectation that, a larger scale system could incorporate a simple air-to-air heat recuperator to use the air exiting the heat exchanger to preheat the inlet air to reduce the penalty losses from the fluidizing gas even further.

Testing is still ongoing at the NSTTF with the goal to slowly ramp up temperatures to the design test conditions listed in Table 1 for the HSP 45/60 particles. At design conditions with the 287µm HSP 45/60 particles, at  $\rho_p = 3610 \text{ kg m}^{-3}$ ,  $T_{p,in} = 600^\circ\text{C}$ ,  $\dot{m}_p = 0.2 \text{ kg s}^{-1}$ ,  $T_{g,in} = 400^\circ\text{C}$ ,  $\dot{m}_g = 0.002 \text{ to } 0.004 \text{ kg s}^{-1}$ ,  $T_{sCO_2,in} = 400^\circ\text{C}$ ,  $\dot{m}_{sCO_2} = 0.2 \text{ g s}^{-1}$ , the reduced order model predicts heat exchanger performance of  $U \approx 500 \text{ W m}^{-2} \text{ K}^{-1}$ ,  $\epsilon_{HX} \approx 0.81$ , mean  $q''_w \approx 23 \text{ kW m}^{-2}$  in the region of the fluidized bed and vertical sCO<sub>2</sub> channel flows. The test plan includes exploring off-design conditions to investigate how variation in parameters such as  $d_p$ ,  $\dot{m}_g/\dot{m}_p$ , and  $T_{p,in}$  can improve understanding of performance and provide calibration for improving design models for potential future scale-up of narrow-channel counterflow fluidized bed heat exchanger. In a larger-scale system for

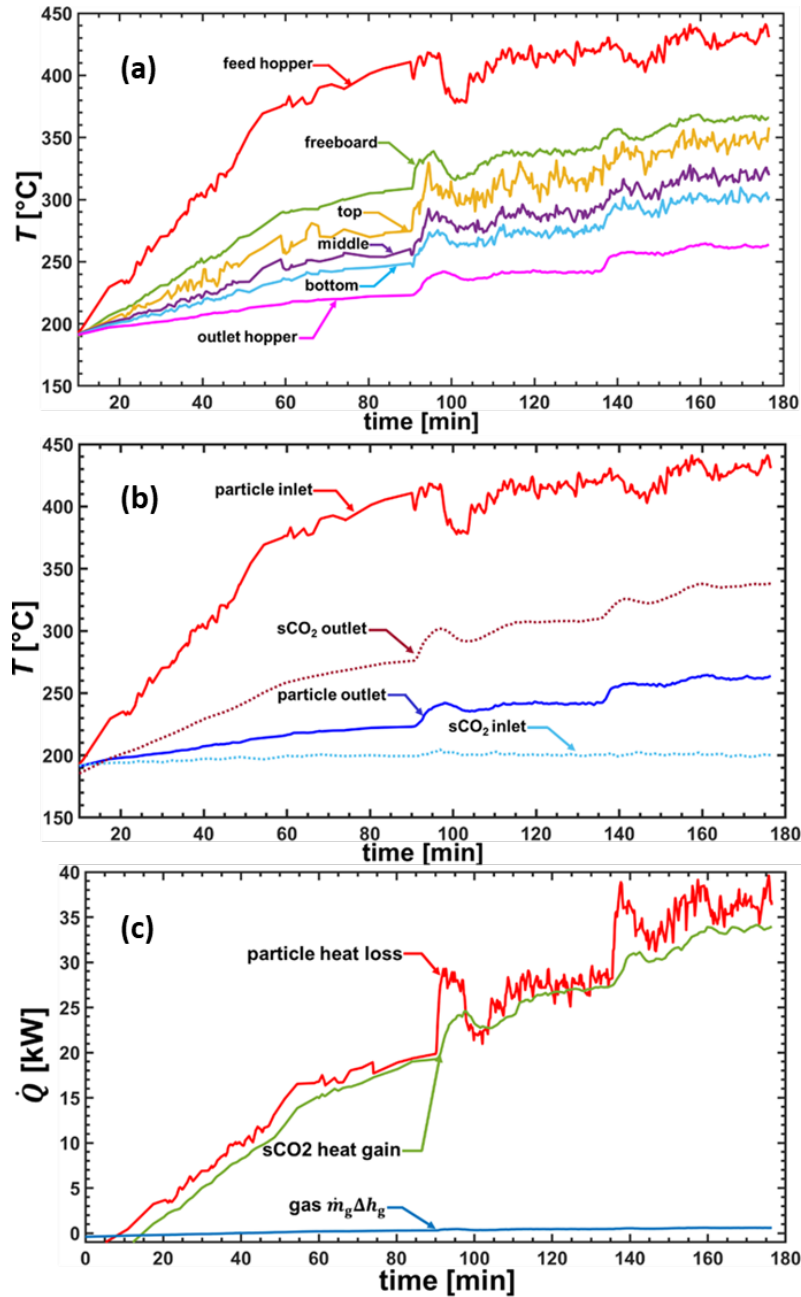


**Figure 5.** a) Average particle temperatures in the feed and outlet hopper, the freeboard zone, and across the instrumented channels in the fluidized-bed, particle-sCO<sub>2</sub> heat exchanger during testing at the NSTTF. Flow conditions followed those listed in the third column of Table 1 with  $\dot{m}_p \approx 0.1 \text{ kg s}^{-1}$  for the first 90 mins,  $\dot{m}_p \approx 0.15 \text{ kg s}^{-1}$  for the next 50 min and the design flow rate  $\dot{m}_p \approx 0.2 \text{ kg s}^{-1}$  for the final 40 min. b) Average  $T_{p,in}$  leaving the feed hopper,  $T_{p,out}$  entering the outlet hopper, and  $T_{sCO_2,in}$  and  $T_{sCO_2,out}$  during the same tests. c) Energy balance in particle-sCO<sub>2</sub> heat exchanger showing the heat transferred from the solid particle flow, into the supercritical carbon dioxide, and fluidizing gas.

## 4. Conclusion

A 40-kW<sup>th</sup> particle-sCO<sub>2</sub> narrow-channel counterflow fluidized bed heat exchanger has been designed and manufactured to demonstrate the heat transfer benefits of mild fluidization of particles compared to state-of-the art moving packed-bed heat exchangers. The 316 stainless-steel prototype heat exchanger comprises 12 channels over 0.56 m high, 0.2 m wide, and 0.0105 m deep and has shown that it can be filled uniformly and operate in a particle-gas

counterflow bubbling arrangement with relatively uniform particle inventory across all instrumented channels. Early test results with particle inlet temperatures to 440°C have indicated that vertical particle dispersion particularly in the upper regions of the narrow-channel fluidized beds reduces the temperature driving force from initial model predictions that neglect vertical dispersion. Increasing particle mass flow rates significantly reduce the impact of dispersion on heat transfer. Despite these challenges, at the design flows of  $\dot{m}_p = 0.2 \text{ kg s}^{-1}$ ,  $\dot{m}_{\text{sCO}_2} = 0.2 \text{ kg s}^{-1}$ , and gas flows  $\dot{m}_g \approx 0.005 \text{ kg s}^{-1}$ , the prototype heat exchanger is able to transfer  $\dot{Q}_{\text{sCO}_2} \approx 34 \text{ kW}_{\text{th}}$  at an overall heat transfer coefficient  $U = 227 \text{ W m}^{-2} \text{ K}^{-1}$  at highest intermediate inlet temperatures  $T_{p,\text{in}} \approx 440^\circ\text{C}$  and  $T_{\text{sCO}_2,\text{in}} = T_{g,\text{in}} = 200^\circ\text{C}$ . It is expected that, at test design conditions with CARBO HSP 45/60 particles, the demonstration heat exchanger can achieve  $U$  approaching  $500 \text{ W m}^{-2} \text{ K}^{-1}$  with an effectiveness  $\varepsilon_{\text{HX}} \approx 0.81$  and a mean wall heat flux in the fluidized region of  $q''_w \approx 23 \text{ kW m}^{-2}$ . Further testing at higher temperatures will be compared with the predicted performance and to obtain data for the improvement of existing design models to better predict and design fluidized bed heat exchangers. Testing the 40-kW<sup>th</sup> fluidized bed particle-sCO<sub>2</sub> heat exchanger at design and off-design conditions will show a clear pathway to demonstrating the heat transfer improvements associated with mild particle fluidization and achieving DOE cost targets for the future scale-up of narrow-channel fluidized bed heat exchangers.

## Competing interests

"The authors declare no competing interests."

## Author Contributions

"Winfred J. Arthur-Arhin [Conceptualization of this study, Methodology, Software, Data curation, Writing- original draft preparation, editing ], Jesse R. Fosheim [Conceptualization of this study, Methodology], Keaton J. Brewster [Data curation, writing - proofing], Azariah Thompson [Methodology], Kevin J. Albrecht [Methodology, Data curation], Dereje Amogne [Methodology], and Gregory S. Jackson1 [Data curation, conceptualization of this study, methodology, writing]."

## Data availability statement

The data presented in this study is based on proprietary design owned by Vacuum Process Engineering. Due to the confidential nature of the design, data is not publicly available, but for research purposes, interested parties can contact the corresponding author, Gregory S. Jackson.

## Funding

This work has been supported by the US DOE Solar Energy Technology Office, under award # DE-EE0008538. The authors thank DOE program manager Shane Powers and former program manager Mark Lausten for their support in this work.

## Acknowledgement

The authors acknowledge Mr. Collin Johnson of VPE for his extensive help in fabricating and delivering the heat exchanger core for this study. The authors also acknowledge Mr. Anthony Evens at Sandia National Laboratory for his assistance in installing and instrumenting the heat exchanger at the NSTTF test facility. The authors also acknowledge Katherine Schubert and Dr. Wanjun Dang who assisted with the narrow-channel testing at the Colorado School of Mines HiTECs Lab.

## References

1. Mehos M, Turchi C, Vidal J, Wagner M, Ma Z, Ho C, et al., "Concentrating Solar Power Gen3 Demonstration Roadmap"., NREL Technical Report #NREL/TP-5500-67464 , National Renewable Energy Laboratory, US Dept. of Energy 2017. DOI: <https://doi.org/10.2172/1338899>.
2. Ho CK, Carlson M, Garg P, Kumar P., "Technoeconomic Analysis of Alternative Solarized s-CO<sub>2</sub> Brayton Cycle Configurations.", *Journal of Solar Energy Engineering-Transactions of the ASME*. 2016;138. DOI: <https://doi.org/10.1115/1.4033573>.
3. Albrecht KJ, Ho CK. "Design and operating considerations for a shell-and-plate, moving packed bed, particle-to-sCO<sub>2</sub> heat exchanger.", *Solar Energy*., 2019;178:331-40. DOI: <https://doi.org/10.1016/j.solener.2018.11.065>.
4. Baumann T, Zunft S, Tamme R. "Moving Bed Heat Exchangers for Use With Heat Storage in Concentrating Solar Plants: A Multiphase Model." *Heat Transfer Engineering*., 2014;35:224-31. DOI: <https://doi.org/10.1080/01457632.2013.825154>.
5. Albrecht KJ, Carlson MD, Laubscher HF, Crandell R, DeLovato N, Ho CK. "Testing and model validation of a prototype moving packed-bed particle-to-sCO<sub>2</sub> heat exchanger.", *AIP Conference Proceedings*, 2020;2303:030002.
6. Keplinger T, Haider M, Steinparzer T, Patrejko A, Trunner P, Haselgrübler M. "Dynamic simulation of an electric arc furnace waste heat recovery system for steam production.", *Applied Thermal Engineering*. 2018;135:188-96. DOI: <https://doi.org/10.1016/j.applthermaleng.2018.02.060>.
7. Yu Q, Yang Y, Wang Z, Zhu H. "Modeling and parameter sensitivity analysis of fluidized bed solid particle/sCO<sub>2</sub> heat exchanger for concentrated solar power plant.", *Applied Thermal Engineering*., 2021;197:117429. DOI: <https://doi.org/10.1016/j.applthermaleng.2021.117429>.
8. Miller DC, Pfutzner CJ, Jackson GS. "Heat transfer in counterflow fluidized bed of oxide particles for thermal energy storage.", *International Journal of Heat and Mass Transfer*. , 2018;126:730-45. DOI: <https://doi.org/10.1016/j.ijheatmasstransfer.2018.05.165>.
9. Fosheim JR, Hernandez X, Abraham J, Thompson A, Jesteadt B, Jackson GS, et al. "Narrow-channel fluidized beds for particle-sCO<sub>2</sub> heat exchangers in next generation CPS plants.", *AIP Conference Proceedings*, 2022;2445:160007.
10. Molerus O. "Heat-transfer in gas fluidized beds 2. Dependence of heat transfer on gas velocity.", *Powder Technology*, 1992;70:15-20.
11. Fosheim JR, Hernandez X, Arthur-Arhin WJ, Thompson AB, Bowen CP, Albrecht KJ, et al. "Design of a 40-kW<sub>th</sub> Counterflow Particle-Supercritical Carbon Dioxide Narrow-Channel Fluidized Bed Heat Exchanger.", In: R. B, editor. *SolarPACES 2021: International Conference on Concentrating Solar Power and Chemical Energy Systems*2021.
12. K. J. Albrecht, H. F. Laubscher, C. P. Bowen, and C. K. Ho, "Performance Evaluation of a Prototype Moving Packed-Bed Particle / sCO<sub>2</sub> Heat Exchanger," Sandia Report, SAND2022-12615, September 2022. DOI: <https://doi.org/10.2172/1887943>.